Self-consistent implementation of anomalous transport closures in a Hall effect thruster model

IEPC-2025-361

Presented at the 39th International Electric Propulsion Conference, Imperial College London, London, United Kingdom
14-19 September 2025

Declan G. Brick* Parker J. Roberts† and Benjamin A. Jorns‡
University of Michigan, Ann Arbor, Michigan, 48109, United States of America

A self consistent closure for the anomalous transport is presented based on the plasma density, neutral density, and electron temperature. This closure, along with an adiabatic heat flux closure along magnetic field lines is implemented in a multi-fluid Hall thruster model. The model outputs for a 9 KW class magnetically shielded Hall thruster are compared to experimental measurements of the centerline plasma properties and performance metrics such as thrust, specific impulse, and efficiency modes as the dependence of the closure upon the selected properties is adjusted. It is found that including neutral density in the model enables the peak electron temperature and performance to be captured, although the electron temperature and ion velocity profiles are unable to be simultaneously placed in the positions indicated by experimental data. The implications of these findings for understanding of the anomalous transport and for improving model fidelity are discussed.

*PhD Candidate, Department of Aerospace Engineering, and brickd@umich.edu.
†PhD, Department of Aerospace Engineering, and pjrob@umich.edu.
‡Associate Professor, Department of Aerospace Engineering, and bjorns@umich.edu.

Nomenclature

$\vec{B}$	= magnetic field
C	= overall scaling coefficient of anomalous transport model.
e	= fundamental charge
$\vec{E}$	= electric field
$\vec{j}_e$	= electron current density
m_e	= electron mass
n_e	= electron number density
$\vec{q}$	= heat flux
Q	= collisional energy transfer
T_e	= electron temperature
$\vec{u}_s$	= velocity of species s
z	= axial position
Z^*	= average ion charge state
$ln(\Lambda)$	= Coulomb logarithim
$\kappa_\parallel$	= thermal conductivity along magnetic field line
$\kappa_\perp$	= thermal conductivity across magnetic field line
μ	= power coefficient of electron density dependence in anomalous transport model.
ν_c	= classical collision frequency
ν_e	= total electron collision frequency
ν_{an}	= anomalous collision frequency
ρ	= power coefficient of neutral density dependence in anomalous transport model.
τ	= power coefficient of electron temperature dependence in anomalous transport model.
ϕ	= electrostatic potential
ω_{ce}	= electron cyclotron frequency

I. Introduction

While Hall effect thrusters are one of the most mature and widely flown types of electric propulsion (EP),[1,2] the fully predictive modeling of these devices remains an outstanding challenge. This capability gap stems primarily from the fact that there are aspects of momentum and energy flux in Hall thruster plasmas that are non-classical in nature. These effects could in principle be captured by fully kinetic representations, but even with recent gains in parallel computing these are computationally cost prohibitive for engineering applications.[3–5] Conversely, these poorly understood processes prohibit the use of reduced fidelity formulations.

In light of this limitation, the most popular approach for thruster modeling is to represent the non-classical processes with effective transport coefficients. This procedure is typically accomplished with an "anomalous" collision frequency (ν_{an}) in the electron momentum equation of a fluid model. While this is an rigorous method for introducing non-classical levels of momentum flux in these devices,[6] adopting this approach inherently invites a problem of closure. The introduction of an unspecified parameter opens the system of equations as the number of plasma properties exceeds the number of governing equations.

In an attempt to address this problem, previous authors have proposed a number of self-consistent closures, i.e. models that depend on other plasma fluid properties, based on effects such as Bohm-like diffusion,[7] wall collisions,[8,9] shear-suppression,[10–12] turbulence analogs,[13,14] wave driven,[15–18] dimensional analysis,[19] and data driven forms.[20,21] Notwithstanding the extensive effort put forth by the EP community, none of these closures have proved fully predictive across multiple operating conditions and thrusters and the issue of anomalous electron transport remains outstanding.

Despite these outstanding challenges, recent experimental developments have motivated revisiting simple, algebraic closure models for the anomalous transport. The application of incoherent Thomson scattering (ITS) to Hall thrusters has allowed, for the first time, direct and non-invasive measurement of the electron properties[22–24] and effective collision frequency[25,26] in the near-field. These measurements showed the unexpected result that the electron temperatures were approximately a factor of two higher than the values previously measured with probe-based techniques. These measurements also revealed an axial anomalous collision frequency profile that is more spatially relaxed than previously estimated.[23] In an effort to explain these results, we have showed in recent work that previous models may have been overestimating the heat flux across field lines by representing it as non-classical.[27] Similarly, setting the heat flux to zero along field lines allows for simulations employing the empirical profiles to match centerline, radial, and global thruster data.[28]

These findings have major implications for evaluating potential closure models. In particular, a key feature that we demonstrated in our previous work is that with a classical model for perpendicular heat flux and adiabatic parallel energy transport, the anomalous collision frequency for the electron momentum can be more relaxed as a function of axial position in the thruster than the variation that previously been expected in fluid-based model. This result is confirmed by experiment[23] and opens the possibility that closure model that depends simply on the spatial variation of conventional background plasma properties like density and temperature may be sufficient.

To this end, in previous work[29] we showed that assuming a scaled form of the electron-ion collision frequency in a fluid model yielded strong agreement with key experimental measurements of the ion acceleration. These exploratory simulations failed, however, to capture peak temperatures and global performance metrics. Given these initial promising results, the need is apparent to expand on these previous studies, systematically evaluating simplified algebraic closures to better capture plasma behavior and thruster performance.

The goal of this paper is to evaluate the dependencies of density, neutral density, and temperature. In Section II, we outline the thruster principle of operation, multi-fluid model, and forms for closure we explore. Section III describes the thruster an dataset we use to evaluate model performance. We then present our key results in Sec. IV, comparing simulation to experimental measurement. Finally, in Sec. V, we discuss our findings as they relate to our understanding electron transport.

II. Modeling Approach

In this section we first describe the operation of a Hall thruster and its key regions. We then detail the computational model we used to investigate our self-consistent closure. We conclude with an overview of the

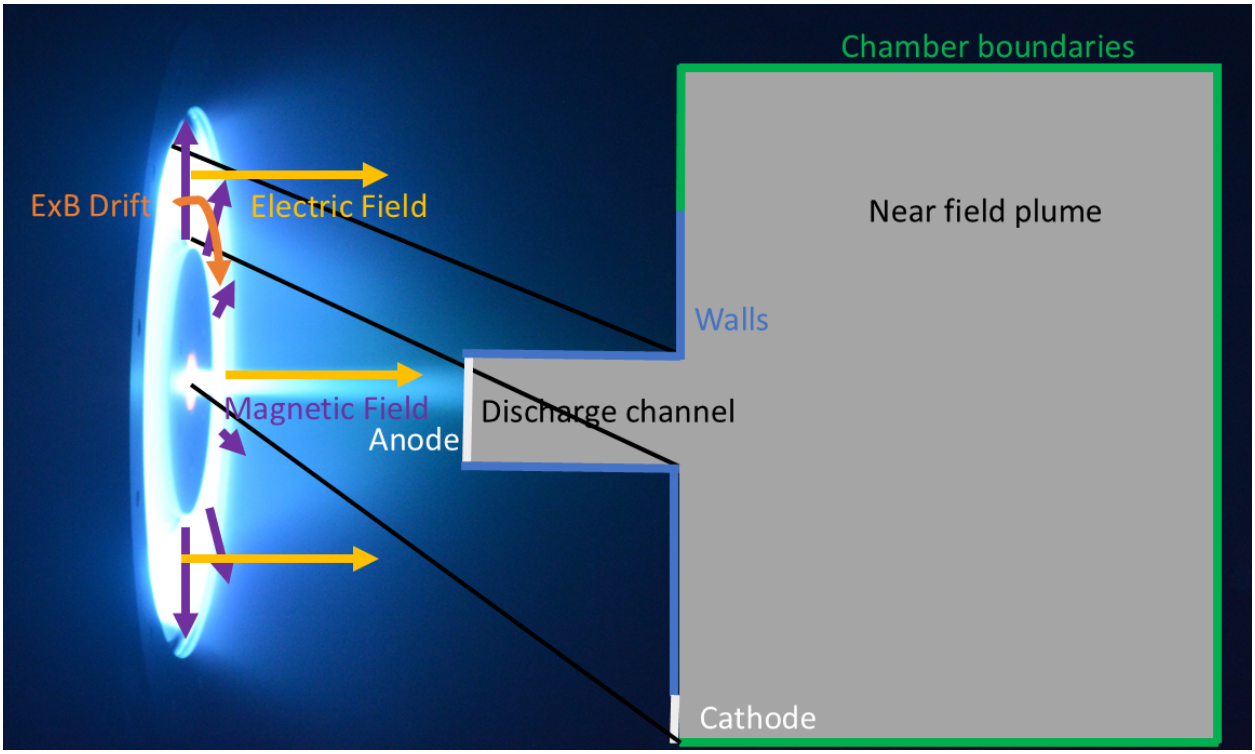

Figure 1. H9 thruster in operation with notional computational domain and key components.

closures to the electron heat flux and anomalous collision frequency employed in this work.

A. Hall Thruster Principle of Operation

Figure 1 shows a cross-section of a Hall effect thruster, highlighting the critical fields and regions of the thruster we simulate. The axial electric field and radial magnetic field form an azimuthal drift for the electrons. Key regions include the discharge channel bounded by an anode and thruster walls; the near field plume, which is bounded by the thruster poles; channel and cathode exits; and the ambient chamber.

Hall thruster operation centers around the radial magnetic field generated by permanent or electromagnets and the axial electric field set up by establishing a potential difference between the anode and cathode. These two fields interact to trap electrons in an E×B drift. The confinement of the electrons produces a step potential drop which then heats the electrons through resistive "Ohmic" heating. Neutral gas is flowed through the anode and down the discharge channel where it is ionized upon contact with the electrons. These ions are then rapidly accelerated due to the sharp electric field, producing thrust. The ionization and scattering collisions with heavy species allow the electrons to migrate across magnetic field lines to the anode, completing the electrical circuit. Quasineutrality is maintained in the channel by replenishment of the trapped electrons via ionization and downstream by continuous emission of electrons from the thermionically emitting cathode that follow ions downstream.

B. Multi-fluid Hall thruster model description

We utilize in this investigation Hall2De, a two dimensional axisymetrric multi-fluid model developed by the Jet Propulsion Laboratory (JPL). As the governing equations, boundary conditions, and numerical implementation have been described elsewhere,[30–33] we only provide an overview of the code. We note as well that while JPL has recently developed a hybrid PIC approach,[34] we make use of the full fluid treatment of the plasma.

In this version of the code, the ions are represented as multiple fluid populations to account for the slow rate of equilibration between the channel and cathode ion beams. A continuity, momentum, and energy equation is solved for each population. Neutrals are treated using a viewfactor approach where they are

assumed to travel in straight line trajectories until they are ionized, reflect off a wall, or leave the domain. Binning of the velocity space enables this approach to account for the disproportionate effects of ionization on the low energy neutral tail. Both heavy species are considered unmagnetized and so are evaluated on a rectilinear axial-radial mesh. Electron continuity is treated via quasi-neutrality which allows for the electron density to be solved as the sum of the densities of ion populations.

Electron momentum is treated by neglecting electron inertia to arrive at the generalized Ohm's law

$$\frac{m_e(\nu_c + \nu_{an})}{e}\vec{j}_e = e\nabla(n_e T_e) - en_e\nabla\phi - \vec{j}_e \times \vec{B} - \frac{em_e n_e}{\nu_e}\Sigma_{s\neq e}(\nu_c + \nu_{an})\vec{u}_s, \tag{1}$$

where m_e is the electron mass, e is the fundamental charge, $\vec{j}_e$ is the electron current density, ν_c is the classical collision frequency, which accounts for ionization, Coulomb, electron neutral scattering, and wall collisions, ν_{an} is the anomalous collision frequency, n_e is the electron density, T_e is the electron temperature (in eV), ϕ is the electrostatic potential, $\vec{B}$ is the magnetic field, and $\vec{u}_s$ is the velocity of ion species s. Physically, Eqn. 1 identifies four drivers of electron current: collisions with other species, the electron pressure, the electric field, the magnetic field, and interactions with ions (such as the main ion beam accelerating electrons from the cathode plume).

Due to the magnetized nature of the electrons in Hall thrusters, the transport coefficients can differ widely between motion across and along magnetic field lines, which can introduce numerical diffusion. To resolve this issue, Hall2De solves electron properties on a magnetically field aligned mesh. An additional benefit of this approach is the ease of implementation of different transport mechanisms parallel and perpendicular to the magnetic field. For closure of Eqn. 1, while the magnetic field is set by thruster design and the ion properties are self-consistently solved for, we need expressions for the potential and electron temperature. The potential can be solved by combining Ohm's law with current conservation which is described in detail in Ref. 31. The temperature is solved using the electron energy equation

$$\frac{3}{2}en_e\frac{\partial T_e}{\partial t} + \nabla\cdot\left(-\frac{5}{2}\vec{j}_e T_e + \vec{q}\right) = \vec{E}\cdot\vec{j}_e + Q - \frac{3}{2}T_e\nabla\cdot\vec{j}_e, \tag{2}$$

where $\vec{q}$ is the electron heat flux, $\vec{E} = -\nabla\phi$ is the electric field, and Q is a term that represents energy losses due to collisions with other species. Physically, the left side consists of the time rate of change of the electron energy and the energy fluxes, which consists of a convective and heat flux. The right side represents sources and sinks of energy which from left to right are the Ohmic heating, collisions with other species, and a flux like term that arises out of combination of the energy equation with Ohm's law to arise at the specific formulation shown here.[35] The heat flux does need to be specified, which we discuss later in this section, but Eqn. 2 otherwise closes the system of equations, representing a complete model.

With our complete set of equations, there are remaining input parameters in the multifluid approach to the ions, the cathode input properties, the thermal boundary conditions, and simulation operation. Table 1 give the values of these parameters in this work. We employ two ion fluid populations with ions born at or above 240V assigned to the beam population and those below assigned to the cathode population. This potential correctly sorts the ions born in the ionization and acceleration regions into the beam population and all others into the cathode population. Three charge states are modeled as experimental results suggest negligible presence of higher charge states in the thruster we model in this effort.[36] For the hollow cathode, we specify the mass flow as a fraction of the anode flow, inflow ion and electron temperatures, and set the potential to 0V, meaning that all potentials in the simulation are referenced to the cathode, representing a body-tied electrical configuration. The cathode input properties are based on standalone measurements of cathode properties.[37] For thermal boundary conditions, the electron temperature is set using a Dirichlet condition of 2.5 eV at chamber boundaries, which is in the middle of the typical range of far-field temperatures for Hall thrusters.[31] For the heavy species thermal conditions when colliding with walls, the wall temperature is set based on experimental thermocouple measurements. The timestep was set at the highest possible stable value of 50 ms. The results presented in the following represent time-averages of all the plasma quantities of interest over an averaging window of 1.5ms which begins after the model reaches a steady state discharge current oscillation.

C. Energy Closure

The heat flux in Eqn. 2 represents a closure problem in that it requires another governing equation. However, adding such an equation would introduce a new variation so Hall thruster models typically use a Spitzer-Harm

Table 1. Hall2De Simulation Parameters

Parameter	Value
Operating Condition	Kr300V15A
Number of ion fluids	2
Discriminating Potential	240 V
Maximum charge state	3
Cathode flow fraction	7 %
Cathode electron temperature	3.0 eV
Cathode ion temperature	0.1 eV
Cathode potential	0 V
Far field electron temperature	2.5 eV
Wall temperature	500 °C
Timestep	50 ns
Simulation duration	1.5 ms

formulation to express the heat flux in terms of the temperature gradient and thermal conductivity[38,39]

$$\vec{q} = -\kappa \nabla T_e, \tag{3}$$

where κ is the thermal conductivity. Physically, this form describes energy flowing down the temperature gradient with the rate at which it does so controlled by the conductivity, which is a property of the medium. For magnetized electrons, the value of the conductivity differs parallel and perpendicular to field lines with the values[39]

$$\kappa_{\parallel} = a(Z^*)\frac{n_e T_e}{m_e \nu_e} \qquad \kappa_{\perp} = b(Z^*)\frac{n_e T_e \nu_e}{m_e \omega_{ce}^2}, \tag{4}$$

where $\parallel$ refers to the parallel direction along field lines, $\perp$ refers to the perpendicular direction across field lines, a and b are coefficients tabulated as a function of the average ion charge state $Z*$ in Ref. 39, ν_e is the electron collision frequency, and ω_{ce} is the electron cyclotron frequency. Physically, collisions decrease conductivity along field lines but increase it across them.

The form of ν_e used in the calculation of the perpendicular thermal conductivity has traditionally included the anomalous collision frequency.[31,40–46] Here however, we only use the classical collision frequency in the determination of $\kappa_{\perp}$. We adopt this approach following our investigation in Refs. 27 and.[28] We showed in these previous works that not only was there no theoretical justification for incorporating the anomalous momentum collision term in the thermal conductivity but that modeling results indicate this inclusion can artificially broaden the temperature profiles.[27] Along field lines, we set the thermal conductivity of the electrons to zero. We use this approximation as we showed in Ref. 28 that removing the heat flux along field lines allowed models to better approximate the two-dimensional spatial distribution of electron temperature along magnetic field lines. Taken together then, we can express our formulation for heat flux in this work as the heat flux we employ is expressed as

$$q_{\parallel} = 0 \qquad q_{\perp} = -b(Z^*)\frac{n_e T_e \nu_c}{m_e \omega_{ce}^2}\nabla_{\perp} T_e. \tag{5}$$

D. Anomalous Collision Frequency Closure

The goal of a closure model for the anomalous collision frequency is to express ν_{an} in terms of the other plasma properties. To motivate what key dependencies we should consider, we note the growing theoretical and experimental evidence which has shown that wave-particle interactions may be a driving factor enhancing transport in Hall thrusters.[18,47–52] The first-principles treatment is to identify the dominant instability and average over the velocity phase space to arrive at a closed form[6] as done in Refs. 16 and 18.

In this work, however, we adopt a more qualitative approach based on an intuitive understanding of the key dynamics. We assume that an unspecified wave mechanism enhances transport by removing energy from the electrons and transferring it to the ions resulting in a net axial force towards the anode. We also assume

that neutral damping may play a role in reducing this exchange, for example, as in ion-acoustic turbulence (IAT).[53]

From this picture, we might expect the plasma density, neutral density, and electron temperature to be key parameters. The plasma density is important as more interactions between the electrons and ions would increase the transfer of energy, resulting in a larger net force. Similarly, larger neutral densities would be expected to produce more neutral damping. The electron temperature is important it is the dominant term in the electron energy, which can be seen in the electron Mach number in Hall thrusters is order 0.1, suggesting that the kinetic energy is roughly two orders of magnitude smaller than the thermal energy.

Empirically, our previous work in Ref. 29 closed the anomalous collision frequency by scaling the electron-ion collision frequency due to Coulomb collisions, which is a power-law function of the plasma density and electron temperature. Notably, the electron ion collision frequency approximately correctly places the local minimum in the frequency, a feature that is critical for capturing the sharp ion acceleration.[54] Our self-consistent implementation of this model showed that it was able to capture this feature in a model to within a scaling coefficient, justifying this approach.

In this work, we expand upon the original approach by adjusting the powers of the plasma properties in the closure:

$$\nu_{an} = 2.9 \times 10^{-12} ln(\Lambda) C \frac{n_e^{\mu}}{n_n^{\rho} T_e^{\tau}}, \tag{6}$$

where $ln(\Lambda)$ is the Coulomb logarithm, n_n the neutral density, and μ, ρ, τ the coefficients of the plasma density, neutral density, and electron temperature that we adjust in this work. We note that $\mu = 1, \rho = 0, \tau = 1.5$ recovers the Coulombic electron-ion collision frequency. Physically, the dependencies reflect the fact that we expect plasma density to increase transport interactions and neutral density to reduce them, while at larger electron temperatures we expect the loss of some energy to be less impactful. These coefficients are adjusted to investigate their effect on the model output.

III. Dataset for Model Evaluation

In this section we first describe the thruster we model. Included in this description are the sources and experimental quantities we compare to. We conclude with an outline of our calibration of the scaling coefficient C in the anomalous collision frequency.

A. Thruster and Data

In this work we employ the H9 (Figure 1), a 9-kW class Hall thruster jointly developed by the University of Michigan, NASA Jet Propulsion Laboratory (JPL), and the Air Force Research Laboratory, for evaluating our modeling results. The H9 is magnetically shielded and features a centrally mounted cathode. We employ this thruster as it was designed as a testbed for investigating thruster physics and has been extensively characterized in the near decade since its inception.

Table 2 gives the operating condition for that we consider in this work. We also include key efficiency modes: the mass efficiency which describes the ratio of ion mass flow rate to neutral mass flow rate, the beam efficiency which describes the ratio of ion current to total current, and the divergence efficiency which describes the square of the ratio of axial current to total current.[36] All performance metrics are pulled from Ref. 36.

Figure 2 plots the one dimensional data along channel centerline. In this work we employ the ion velocity measurements from Ref. 55 and the electron temperature measurements from Ref. 25. In the ion velocity profile we observe a sharp ion acceleration as the velocity increases by an order of magnitude over a distance of roughly one fourth the length of the channel. This trend is consistent with the steep potential drop caused by confinement of electrons by the magnetic field. In the electron temperature we observe a maximum value near the channel exit that is driven by Ohmic heating in the region of the electric field. The temperature then falls off downstream as the lower electric field does not heat the electrons as much as upstream and the plume expands. We note that while we do not fully resolve the peak in electron temperature, we do not expect the peak value to be more than 5 eV higher than the furthest upstream point. This expectation is based on the fact that the electric field upstream is weaker and the electrons lose energy due to ionization in the channel. We will compare model outputs to this dataset to evaluate the efficacy of our closure.

Table 2. Experiential Performance Metrics

Measurement	Value
Propellant	Krypton
Discharge voltage	300 V
Discharge current	15±0.1 A
Mass efficiency	82.6±3.4 %
Beam efficiency	82.3±3.1 %
Divergence efficiency	81.6±0.8 %

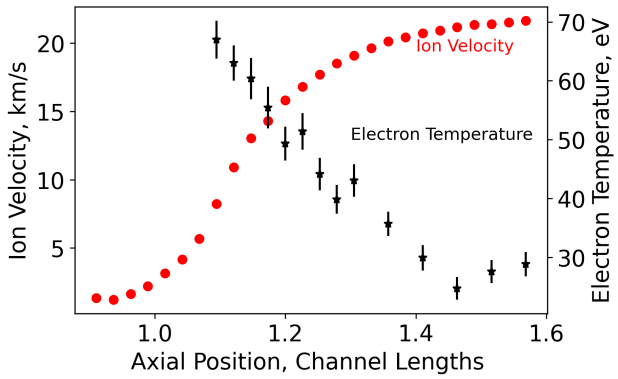

Figure 2. Ion velocity and electron temperature along channel centerline for H9 operation on krypton at 300 V and 15 A.

B. Approach to model calibration

To compare models to our measurements from the H9, we follow a procedural approach based first on identifying the best scaling coefficient, c, for a given set of exponents in Eq. 6. As our metric for quantifying goodness of fit for this initial calibration, we employed the ion velocity profile where adopted the convention of the ion velocity residual (IVR) as[17]

$$IVR = \sqrt{\frac{\int_{z_u}^{z_d}(u_{i,model}(z) - u_{i,EXP}(z))^2 dz}{\int_{z_u}^{z_d} u_{i,EXP}^2 dz}}, \tag{7}$$

where z is the axial position and u_i is the ion velocity with the subscripts u and d denoting the upstream and downstream bounds of the measurement. The IVR was designed to be comparable to a percentage with a value of 0.1 representing 10% error. In an analogous manner, we can also calculate the temperature residual (TR) for the electron temperature profile as

$$TR = \sqrt{\frac{\int_{z_u}^{z_d}(T_{e,model}(z) - T_{e,EXP}(z))^2 dz}{\int_{z_u}^{z_d} T_{e,EXP}^2 dz}}. \tag{8}$$

We will show the values of these residuals in Sec. IV.

In our analysis, we would pick a set of exponents, μ, ρ, τ. and an assumed value for c the closure in our model and then run the simulation until achieving a time-averaged steady-state output for discharge current. We parametrically varied c then looking for the value yielding the minimum IVR. Convergence on the minimum was considered achieved when the change in IVR was around 0.002, as that was the maximum magnitude of run-to-run variation caused by noise in Hall2De's matrix solver. Our results in the following for each closure reflect the simulation with c value corresponding to this case. We note here that we elected to employ IVR as our metric as it historically has been the major driver for evaluating model validity in fluid-based codes.[17,54] This stems from the fact that the rapid acceleration in space of the ion velocity seen in Fig. 2 is one of the most problematic features to re-create for self-consistent models.[54,56]

IV. Results

In this section, we present simulated one-dimensional centerline properties and performance metrics as functions of the model coefficients μ, ρ, and τ. In each case, we vary a single parameter while holding the other parameters constant. We first present results for the variation in the plasma density dependence μ, then the neutral density dependence ρ and finally the electron temperature dependence τ. After presenting the plasma properties of each variation we conclude with the optimal scaling coefficients c as a function of the power law coefficients.

A. Varying the Dependence of the Closure Model on Plasma Density

Figure 3 displays the variation of the electron temperature and ion velocity along centerline as well as the TR and IVR values as a function of μ which is the power of the plasma density in Eq. 6. In this case, we have fixed the other exponents to $\rho = 0$ and $\tau = 1.5$ as these are the values of the original electron-ion model in Ref. 29. Our range of μ values was selected as we empirically found that $\mu \leq -1$ values were unconditionally unstable, and values of $-1 < \mu < -0.5$ and $\mu > 2$ did not yield improved matches to experimental data. In the electron temperature profiles, we see that although the profile shapes are qualitatively consistent with the experimental data, the peak values are 10-20 eV lower than the experimental value. This qualitatively is consistent with the interpretation that the electron ion model is not driving sufficient electron heating. The plot of the temperature residual has a local minimum of 10% at $\mu = 0$ which suggests that no dependence upon the plasma density produces the best match between the model and experimental temperature. The difference in TR between the best and worse match is around 7%, which is reflective of the slight (¡5eV) changes in the overall temperature profile between cases. Notably, the TR does not have a minimum for the case with the highest peak temperature, which reflects the metric taking the overall fit of the curve into account.

For the ion velocity profiles, all the models capture the approximate magnitude and shape of the ion acceleration with around 0.1 channel lengths variation in the location where the ion acceleration begins. The main difference between results is that for larger values of μ, the acceleration starts further downstream and has a larger final value. In the corresponding IVR plot, this trend manifests as a lower IVR value indicating a better fit to the experimental data. The best case fit is the $\mu = 2.0$ case with an IVR of 11%. We note that the best case IVR value is not for the same coefficient value as the best case TR coefficient.

Figure 4 shows the global metrics as a function of μ variation. The experimental values are plotted as a solid line with the shaded region representing experimental error. For all cases, the mass efficiency increases the with decreasing μ. Generally, this leads to a similar trend in the discharge current, with the notable exception that $\mu = -0.5$ exhibits a similar discharge current to $\mu = 0.0$ despite a higher mass efficiency. This result can be explained in the beam efficiency, which decreases closer to the experimental measurement as μ decreases until the efficiency increases again at $\mu = -0.5$. This trend implies that the anode is not collecting as much electron current and the increased mass efficiency is resulting in more ions downstream. Finally, we observe a similar trend in the divergence efficiency as the beam efficiency. In all cases, the model is not able to match all four experimental quantities, although we note that a few cases approach within 1% of the mass and divergence efficiency.

B. Varying the Dependence of the Closure Model on Neutral Density

Figure 5 plots the centerline plasma properties for increasing values of ρ, which represents an increasingly inverse dependence on neutral density. In this case, we have fixed the other exponents to $\mu = 0.0$ and $\tau = 1.5$ as we first want to explore the effect of neutral density independent of the plasma density and $\tau = 1.5$ is the value of the original electron ion collision frequency. Similar to the μ variation, we found empirically that for $\rho > 1$, the model is unconditionally unstable. We do not present results for $\rho < 0$ here as they were similar to $\mu > 0$ values.

In the electron temperature results, we observe again that the electron temperature profiles exhibit qualitatively similar shapes to the experimental data. The peak value of electron temperature increases with ρ, although the difference in the maximum temperature between $\rho = 0.5$ and $\rho = 0.75$ is less than an eV. A similar trend is observed in the downstream tail of the profile, with downstream values increasing by multiple eV between parameters. For the residual, we observe an increase with ρ that suggests an overall worse fit as the model has a stronger dependence with the neutral density. This trend is not, like in the plasma density

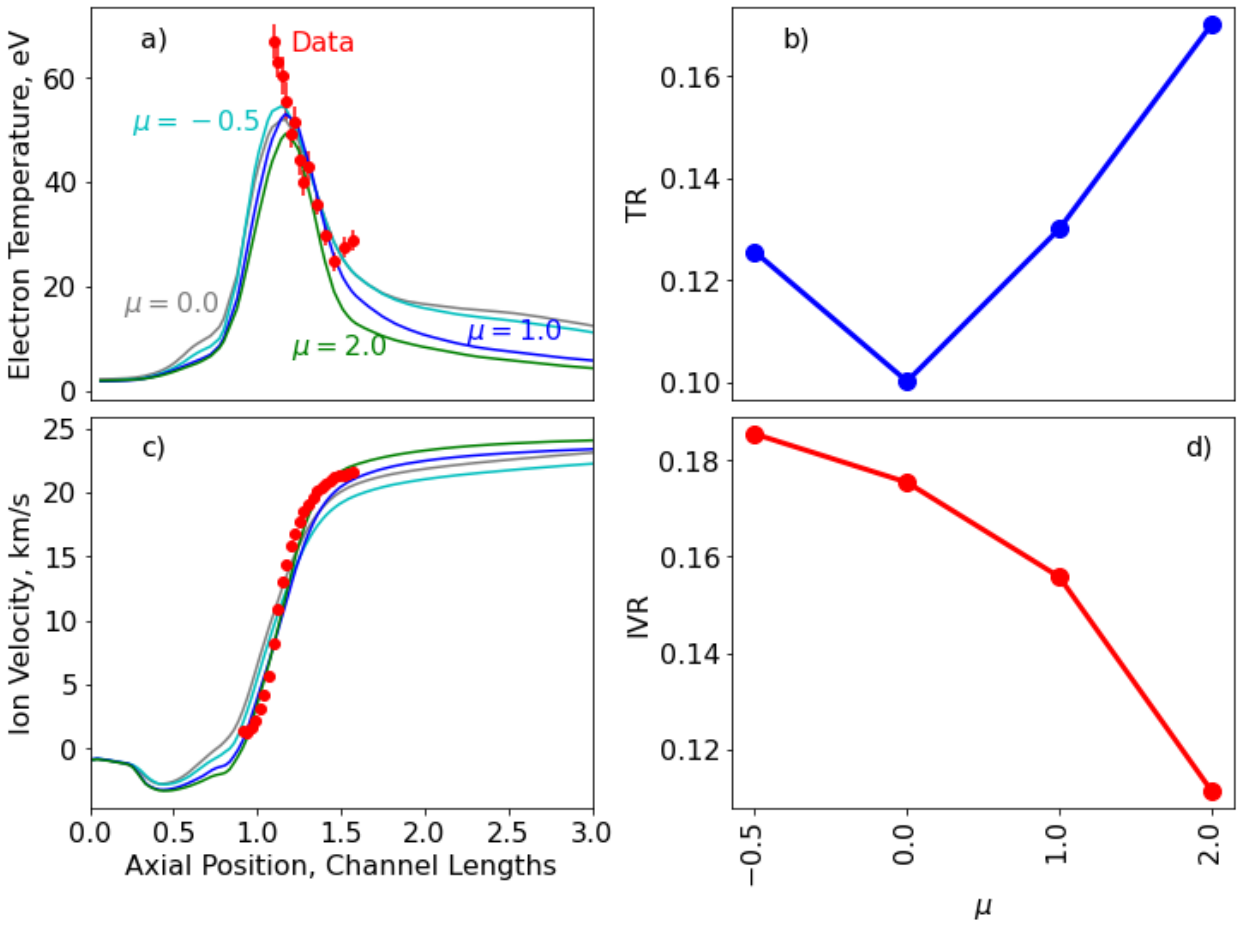

Figure 3. Comparison of a) electron temperature and c) ion velocity along centerline to data and b) TR and d) IVR for various values of plasma density power in the anomalous collision frequency μ. For all cases, $\rho = 0$ and $\tau = 1.5$.

case, commiserate with the trend in the peak temperature. This discrepancy is a result of the increase in temperature downstream of the peak resulting in a worse fit for points in this region even as the peak values are better captured.

For the ion velocity, we find theρ values yield smaller variation than for the μ cases. The most visible change is the decrease in ion velocity approximately halfway through the channel and at the end of the ion acceleration. The velocity values near the downstream of the experimental measurement are lower in the model than in experiment, although the model eventually approaches these values another channel length further downstream. The corresponding trend in the IVR is likewise minor with a difference of only 1% between the minimum and maximum values. We note that the IVR difference between most cases was less than the convergence criteria of 0.2%.

Figure 6 displays the response of the performance metrics with the same variation in ρ as the one dimensional properties. In the discharge current and mass efficiency, we see an increase with ρ for $\rho \leq 0.5$. At the larger values, the mass efficiency peaks at $\rho = 0.75$ while the discharge current peaks at $\rho = 0.5$. The beam efficiency displays an inverted trend to the discharge current as it decreases with ρ for $\rho \leq 0.5$ and has a local minimum at the peak discharge current. All cases underpredict the divergence efficiency with a larger discrepancy between model and experiment at larger values of ρ. Notably, $\rho = 0.375$ simultaneously matches the discharge current, mass efficiency, and beam efficiency with an underprediction in the divergence efficiency by about 5%.

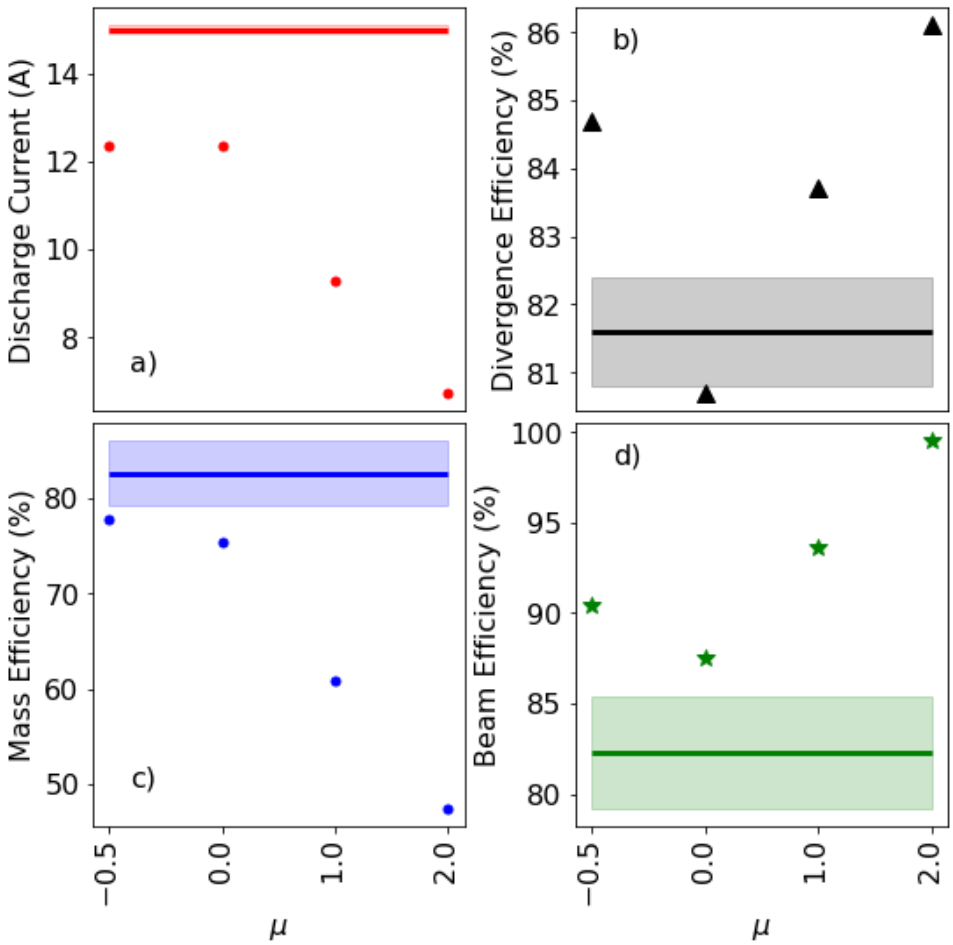

Figure 4. Comparison of a) discharge current b) divergence efficiency c) mass efficiency and d) beam efficiency as a function of plasma density power in the anomalous collision frequency μ. For all cases, $\rho = 0$ and $\tau = 1.5$.

C. Varying the Dependence of the Closure Model on Electron Temperature

Figure 7 shows the one dimensional variation of the plasma properties as a function of the parameter τ which describes the degree to which the model is inversely proportional to temperature. The values for the plasma and neutral density dependencies for all cases are $\rho = 1.0$ and $\mu = 0.5$. This combination is a departure from the preceding subsections where we only allowed one density coefficient to vary at a time. In principle, both coefficients can take finite values, but using the axes of μ and ρ from the subsections would result in twenty parameter combinations per τ value. Considering that the scaling coefficient in each parameter set is optimized, exploring all sets is computationally infeasible. To identify the best combination of μ and ρ we fit time averaged data from a best case simulation to experimental anomalous transport curves from Ref. 28. The best case parameters were taken as $\mu = 0$, $\rho = 0.5$, $\tau = 1.5$ as it had the correct peak temperature, IVR below 20% and the closest match to the global metrics of any case tried. This matching suggested that a ratio of $\frac{\mu}{\rho} = \frac{1}{2}$ was optimal and empirically the $\mu = 0.5$ $\rho = 1$ cases produced better results than lower values of ρ. $\rho > 1$ was not explored due to it behaving as a bound beyond which simulations would not converge. As a final not, although we do not show it here, the trends with τ presented in this section were qualitatively similar regardless of the exact of μ and ρ values.

Figure 7 shows the one dimensional plasma properties and residuals as a function of τ. In terms of the electron temperature profile, we see a decrease in peak temperature with a stronger inverse dependence upon the temperature, represented by an increasing τ. Downstream, this relationship is reversed, with larger values of τ exhibiting modeling results with higher temperatures, corresponding to a shallower temperature gradient in this region. Qualitatively, the shape of the model profile diverges from the shape of the experimental

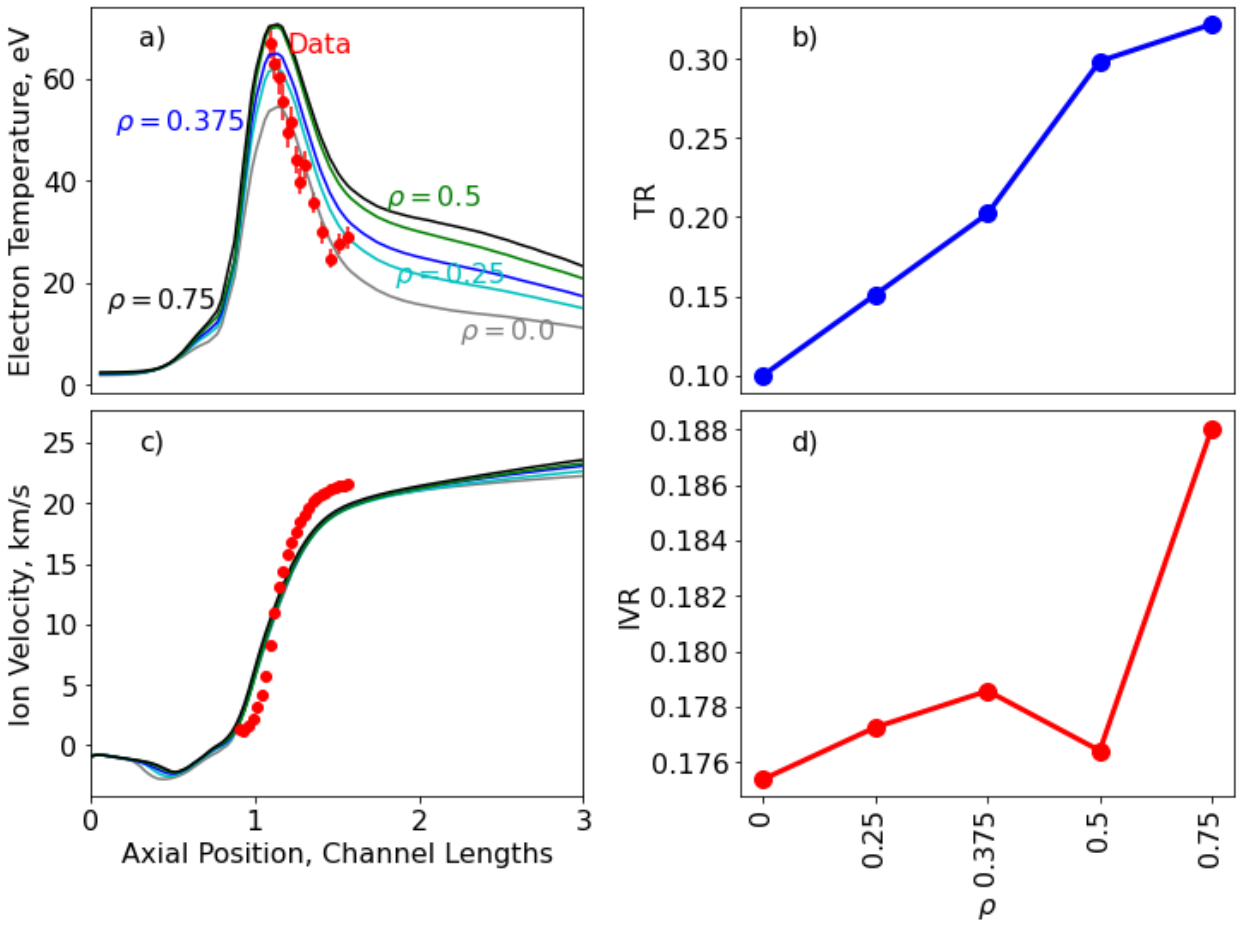

Figure 5. Comparison of a) electron temperature and c) ion velocity along centerline to data and b) TR and d) IVR for various values of neutral density power in the anomalous collision frequency ρ. For all cases, $\mu = 0$ and $\tau = 1.5$.

profile with increasing τ. Compared to the variations in only one density, this variation reaches higher peak temperatures and reproduces the trend of the peak temperature being further downstream than in experiment. For the TR metric, we observe a decreasing residual with increasing τ. This trend reflects the metric favoring correct placement of the peak over the magnitude, which is consistent with the results in the neutral density variation.

The ion velocity curves from 0 to ∼1.25 channel lengths are almost indistinguishable on the plot in shape and magnitude. The notable trend with the temperature dependence is that at larger values of τ the final ion velocity and inflection point at approximately 1.3 channel lengths decrease in magnitude. We note that the difference between the models shrinks further downstream, but the result is that lower values of τ provide a closer match to the ion velocity trace. The value of the IVR reflects this trend with larger values of τ having smaller IVR values.

Figure 8 displays the trends in global performance metrics as a variation of τ that correspond to the simulations used to generate the centerline profiles. Both the beam and divergence efficiencies decrease with increasing τ, with all values of τ giving a beam efficiency within experimental error. The discharge current and mass efficiency trends are similar in dependence, but the mass efficiency between $\tau = 1.5$ and $\tau = 2.0$ are similar while $\tau = 1.0$ and $\tau = 2.0$ exhibit discharge current values within experimental error (0.1 A) of each other. This reflects a smaller dependence on τ in these metrics. Overall, we note that no value of τ can simultaneously match all four performance metrics.

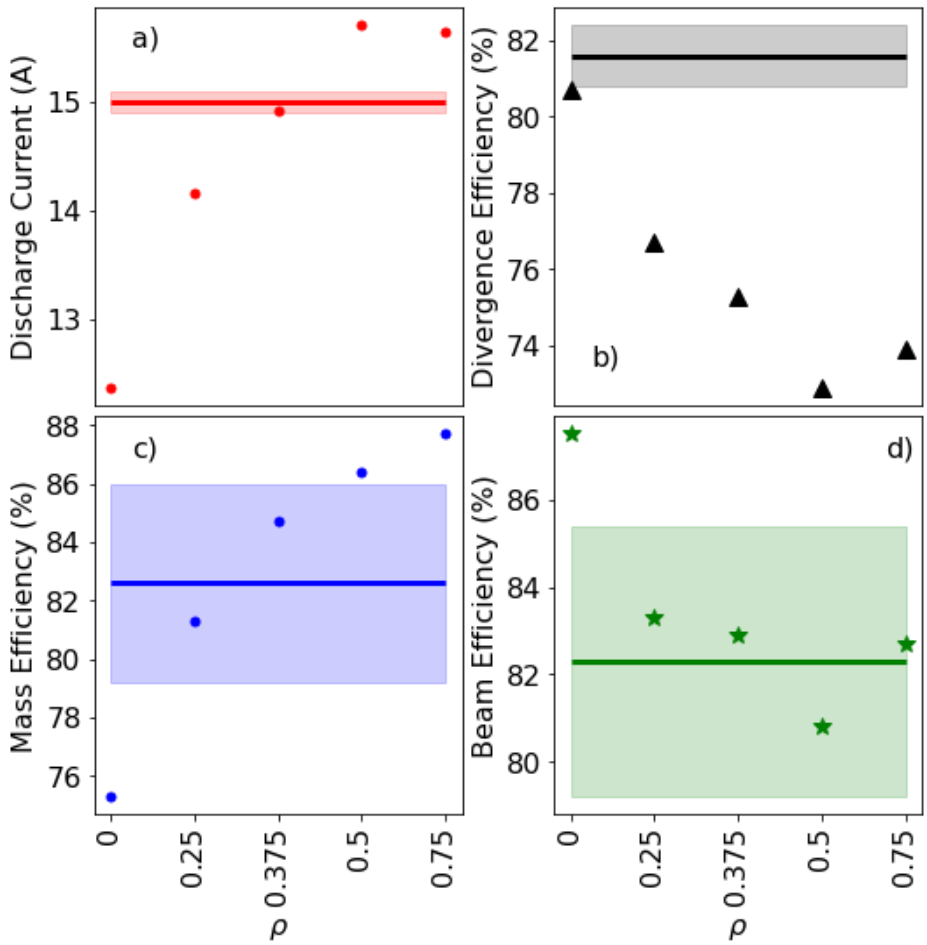

Figure 6. Comparison of a) discharge current b) divergence efficiency c) mass efficiency and d) beam efficiency as a function of neutral density power in the anomalous collision frequency ρ. For all cases, $\mu = 0$ and $\tau = 1.5$.

D. Optimal Coefficients

As mentioned in Sec. II, the one dimensional and performance metrics results in the preceding sections do not have the same c value for each variation of the plasma property dependence. Figure 9 plots the coefficient value that minimizes the IVR for each case. For each variation, we note that they are all generally log-linear. The sign of the slope is related to the proportionality of the parameter with the collision frequency. Specifically, c decreases for the directionally proportional μ coefficient and increases with the inversely proportional ρ and τ parameters. That is as we change any of the coefficients such that for the same value of the property the anomalous collision frequency would be smaller, c increases. We expand more on this result in Sec. V.

E. Summary of Results

In this section we have varied a series of coefficients that affect the dependence of the anomalous collision frequency on the plasma density, neutral density, and electron temperature. The results can be summarized as follows. The variation in plasma density can reproduce the sharp ion acceleration but cannot capture the peak electron temperature or performance metrics. In contrast, the neutral density variation is able to capture the peak temperature and the majority of the performance metrics but places the temperature profile too far downstream and results in a shallower ion acceleration. When the model depends on both densities and the temperature dependency is varied, we observe a modification in the peak electron temperature and near plume ion acceleration with most cases overpredicting the mass efficiency but able to capture the beam

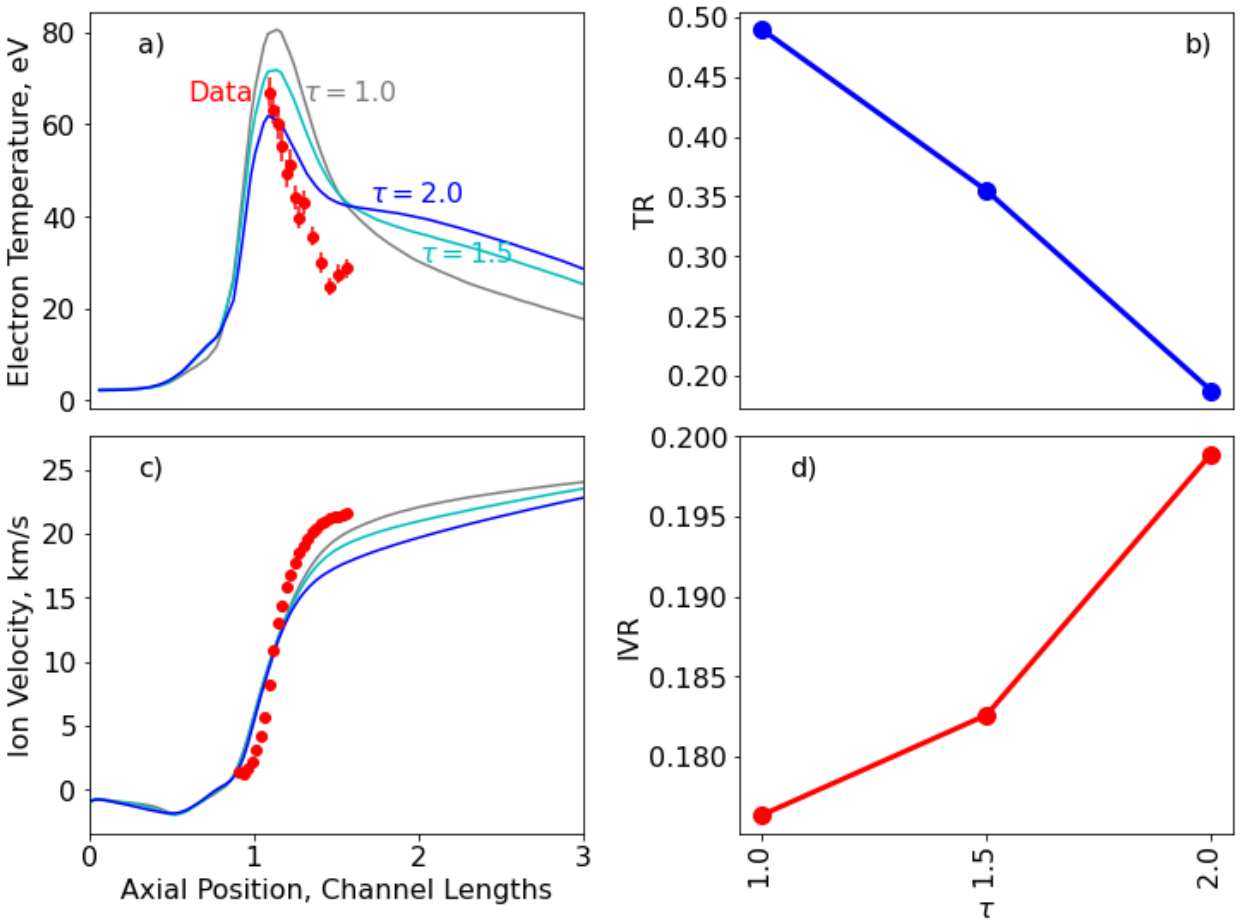

Figure 7. Comparison of a) electron temperature and c) ion velocity along centerline to data and b) TR and d) IVR for various values of electron temperature power in the anomalous collision frequency τ. For all cases, $\mu = 0.5$ and $\rho = 1$.

efficiency. For all cases, we have a divergence efficiency below the experimental value. Finally, we find a log-linear dependence of the overall scaling coefficient c with any variation in the dependency upon the plasma property.

V. Discussion

In this Section we first discuss the trends of global and centerline properties with variations to the density and temperature scalings. We then conclude by examining the implications of the log-linear relationships between our scaling coefficient c and the parameters ρ, μ, and τ.

A. Implications of the Trends of Anomalous Collision Frequency with Density and Temperature

1. *Trends with plasma density scaling (μ)*

Figure 10 plots the collision frequency as a function of the parameter values. We place this result here as observing the trends in the anomalous collision frequency will aid in understanding the trends in the model produced plasma and performance metrics. The key trends we note are 1. in the channel, ν_{an} increases as μ increases, 2. the local minimum generally moves further downstream and has a smaller value as μ increases, and 3. downstream of the local minimum the collision frequency decreases as μ increases.

In addition to the collision frequency a key relation is that of the electric field with the collision frequency

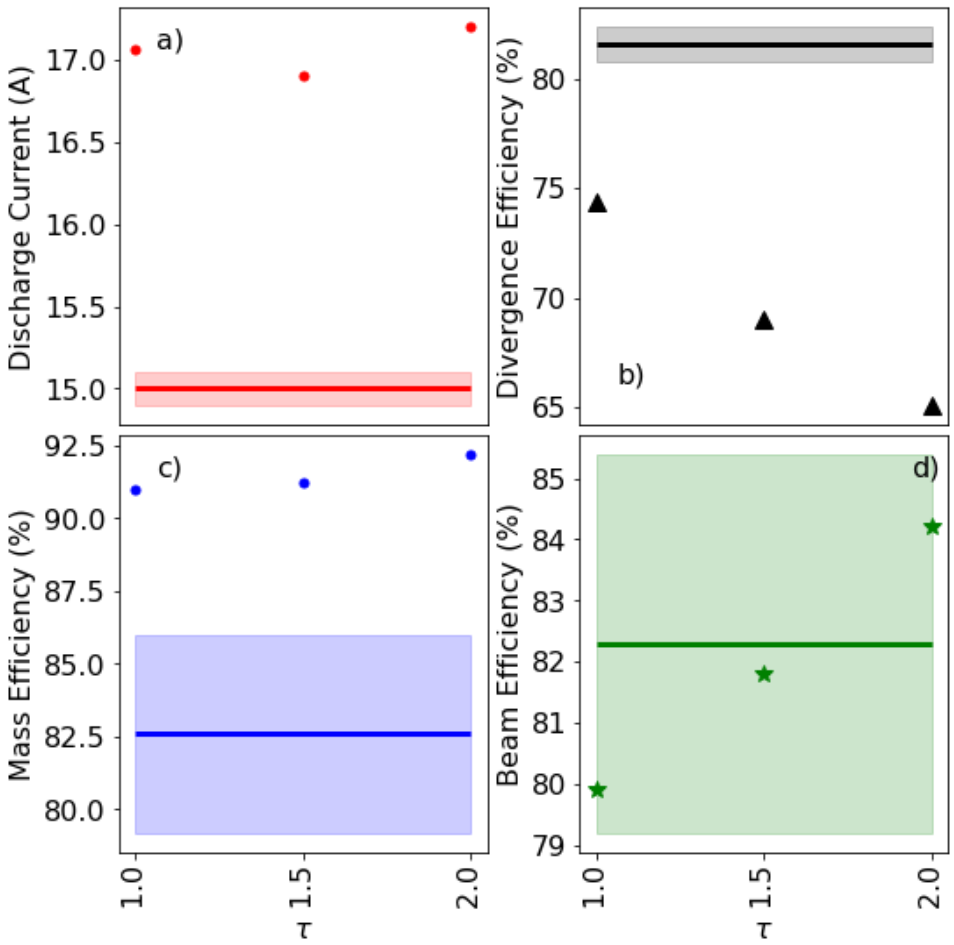

Figure 8. Comparison of a) discharge current b) divergence efficiency c) mass efficiency and d) beam efficiency as a function of electron temperature power in the anomalous collision frequency τ. For all cases, $\mu = 0.5$ and $\rho = 1$.

and the pressure gradient. If we ignore the ion temrs, with are general small, and focus on channel centerline Eq. 1 can be solved for the axial electric field as

$$E_z \propto \frac{1}{\nu_e} j_{ez} - e\nabla_z(n_e T_e). \tag{9}$$

Physically this relation suggests that decreasing the collision frequency produces a larger electric field while increasing temperatures reduce the electric field.

- **Downstream ion velocity increases with exponent** The increase in the downstream ion velocity with μ can be explained in the context of the local minimum in the transport profiles. As larger μ values have smaller local minimums which from examining Eq. 9 results in a larger electric field. This larger field results in more acceleration overall, leading to a sharper ion acceleration and larger final velocity.
- **Downstream electron temperature increases with exponent** The decrease in downstream electron temperature is a result of reduced Ohmic heating from the transport profile. That is, greater values of μ have smaller downstream collision frequencies. As the collision frequency enhances the transport, a reduced frequency results in a smaller electron current density, which suppresses Ohmic heating in the downstream region.
- **Trends in performance metrics**. The location of the ionization is the driver for the trends in performance metrics. To understand this importance we note that the krypton ionization cross section

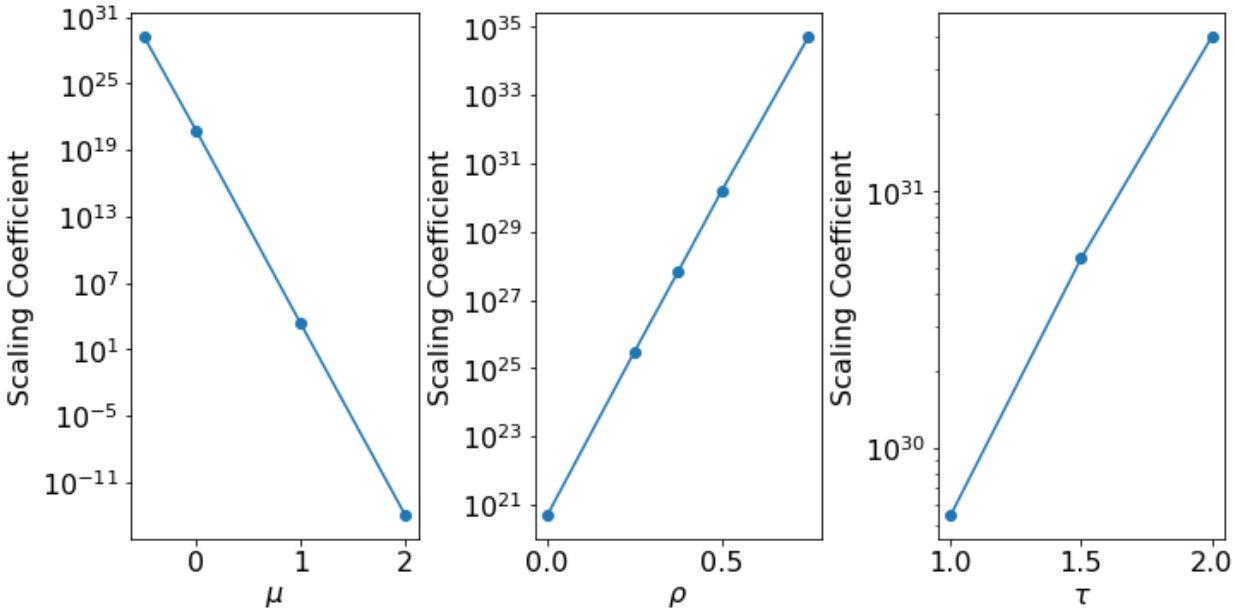

Figure 9. Optimal collision frequency as a function of plasma property dependency parameters. μ is the power of the plasma density, ρ is the power of the neutral density, and τ is the power of the electron temperature. For the μ variation $\rho = 0$ and $\tau = 1.5$, for ρ variation $\mu = 0$ and $\tau = 1.5$, and finally for the τ variation $\mu = 0.5$ and $\rho = 1$.

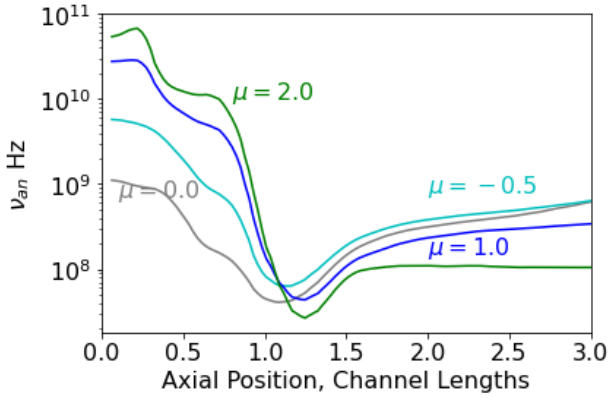

Figure 10. ν_{an} along channel centerline for various values of plasma density power in the anomalous collision frequency μ. For all cases, $\rho = 0$ and $\tau = 1.5$.

increases by an order of magnitude as electron temperature increases from one to ten eV.[57] Therefore, small increases in the electron temperature in regions of low temperature such as before 0.75 channel lengths, can disproportionally increases the ionization. From Fig. 3 we observed that lower values of μ produce larger temperatures in the channel, creating more ionization. The increased ionization explains the increases in the mass efficiency and discharge current. For the beam efficiency, ions born in regions of negative ion velocity will recombine at the anode rather than exiting the thruster to contribute to beam current. The net effect is a decrease in the beam efficiency as electrons generated from increased ionization also reach the anode.

- **Peak electron temperature insensitive to value of μ** The small variation in peak electron temperature is a result of similar Ohmic heating between cases. From the ion velocity plot, we can infer that the electric field in the majority of the channel is relatively small as the ion velocity does not change by orders of magnitude in this region. This inference suggests that the heating in the channel

is driven by variation in the current density. From Fig. 10 larger values of μ will have larger electron velocities as the collision frequency in the channel is larger. However, from the global metrics we know they have lower ionization, which decreases plasma density. These competing effects result in a similar level of current density for each case, explaining the relaitvely constant Ohmic heating.

2. *Trends with neutral density scaling*

Figure 11 plots the variation in the anomalous collision frequency profile with the value of ρ. In contrast to the variation in μ, increasing ρ results in a smaller value of the collision frequency in the channel and a larger value downstream. Additionally, we note that the location and magnitude of the local minimum in the transport profile is similar between all cases.

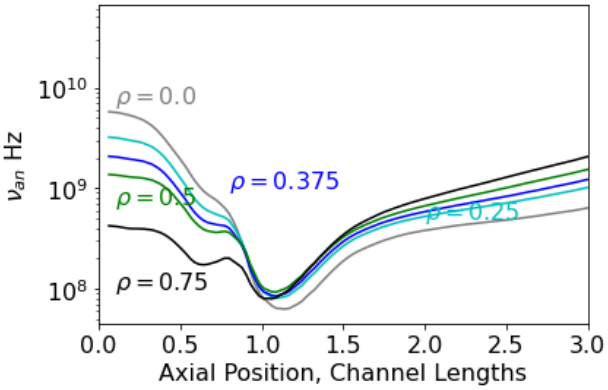

Figure 11. ν_{an} along channel centerline for various values of neutral density power in the anomalous collision frequency ρ. For all cases, $\mu = 0$ and $\tau = 1.5$.

- **Similarities to plasma density trends** Here we highlight the trends of increasing downstream temperature and match in performance metrics with ρ as they have similar underlying causes as was mentioned for the plasma density. For the downstream temperature, we again make the observation that it increases as the downstream collision frequency does, which is driven by higher current densities causing more Ohmic heating in this region. Likewise we observe increased discharge current and mass efficiency with a decreasing beam efficiency. The reasoning her is the same as the plasma density case with slightly higher temperatures in the upstream portion of the channel driving increased ionization. The reader is encouraged to refer to the plasma density variation discussion of these effects for more detail.

- **Insensitivity of ion velocity with value of ρ** The trend of various values of ρ not producing significant change in the ion velocity can be explained by the constant value and location of the local minimum in the collision frequency. From Eq. 9, the constant dip suggests the magnitude and location of the electric field is approximately fixed. Equation 9 also shows a variation with the pressure gradient, which we might expect to vary as the peak temperature changes. However, the increased ionization results in a larger number density. As the neutral density falls off due to acceleration in the region with the increasing electron temperature, this effect offsets the change in temperature gradient, allowing the electric field to remain constant.

- **Peak electron temperature increases with value of ρ** The increase in peak temperature in the variation is an effect of the increased Ohmic heating. As mentioned above in the ion velocity, the electric field is relatively constant between values of μ, so does not explain the difference. Rather the increased Ohmic heating arises from an increase in the current density. Although the collision frequency and therefore electron velocity decreases with ρ, the plasma density increases with improved ionization. This increase in density more than offsets the decrease in the velocity resulting in an overall larger current density and Ohmic heating.

3. Trends with temperature scaling

Figure 12 shows the variation in the collision frequency profile with τ. The trend is that lower values have less collision frequency overall.

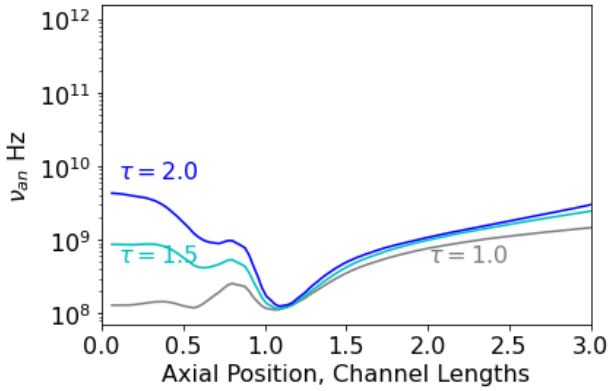

Figure 12. ν_{an} along channel centerline for various values of electron temperature power in the anomalous collision frequency τ. For all cases, $\mu = 0.5$ and $\rho = 1$.

- **Similarities to density trends** Here we note that the change in downstream temperature and global performance metrics can be explained by the same physical mechanisms as in the dnesities variations. The downstream electron temperature is fundamentally driven by the downstream anomalous collision frequency, which when increased causes more Ohmic heating in that region. For the performance metrics, they are governed by the electron temperature in the channel. Compared to the density coefficients however, the electron temperature in the channel changes by a smaller amount for the τ sweep. This effect causes similar ionization for each case, resulting in run to run variation that is typically smaller than experimental error of the metric.
- **Variation in downstream ion velocity** The trend that is most unique to τ is the variation in the ion velocity at the end of the experimental data domain varying by more than 1 $\frac{km}{s}$. This effect is mainly a result of the change in downstream temperature producing a change in the temperature gradient. For example, the electron temperature in the $\tau = 2.0$ case does not fall off as rapidly as a function of z as in the $\tau = 1.0$ case, which is a smaller temperature gradient. From Eq. 9, a shallower decreasing temperature gradient will result in a smaller electric field, explaining the final velocity. Unlike the upstream, the density gradient is in the same direction as the temperature gradient in this region, which is why it does not cancel like the change in temperature gradient not impacting the electric field for the neutral density variation.

B. Insight into the physics of anomalous transport

While the preceding subsection explained the model trends from an Ohm's law perspective, we can also interpret the results using our qualitative picture of the anomalous transport from Sec. II. As mentioned in motivating the plasma density dependence, if the energy is being exchanged between the ions and electrons, we should expect that more charged particles leads to a greater rate of energy exchange and thus transport. In our model, modifying the density variation is analogous to increasing the number of charge carriers. Therefore, the higher peak electron temperature with a decrease in μ is consistent with this qualitative description as the slower rate of exchange allows the electrons to keep more of their energy. For the neutrals, a larger value of ρ increases the effect that neutrals have on suppressing the transport. As the increase in the neutral density allows us to capture the peak temperatures and the discharge current, mass efficiency, and beam efficiency. This result suggests that charged particle interactions with neutrals plays a significant role in anomalous transport. For future efforts that seek to derive closures from first principles, neutral interactions should be considered.

C. Guidance on standards for evaluating future closures

Another key insight our model provides is a path towards resolving non-uniqueness in the ion velocity profile for transport models. The insensitivity to the ion acceleration as large variations occur in the channel collision frequency, in addition to being observed in this work, has been noted as a significant difficulty in developing closure models.[54] In this work we have been able to evaluate the performance of models that mainly differ in their prediction of the channel collision frequency. The reason we have been able to do so is that the channel drives the ionization in these devices. Therefore, our results suggest that to evaluate self-consistent transport closures, the model's prediction of the discharge current, mass efficiency, divergence efficiency, and beam effectively should be evaluated to probe physics of the discharge that the ion velocity profile alone cannot determine.

D. Trends in Scaling Coefficient with Exponent Value

In Sec. IV, we noted that the scaling coefficient C has a log linear dependence with the plasma property coefficients μ, ρ, and τ. This result can be explained by our general observation that in order for a collision frequency profile to yield qualitative agreement with the experimental data, the most critical feature is for the model to exhibit a minimum of the collision frequency at the same location and with the the same magnitude.[29,56] This is intuitive as this feature is the point of maximum cross-field impedance of the device and is therefore expected to be a primary driver for the underlying dynamics in the system.

Preceding under this assumption , for the same value of a plasma property, adjusting the power coefficient can vary the anomalous collision frequency by orders of magnitude. For example, as the plasma density in the channel is on the order of $10^{17}(\frac{1}{m^3})$, changing μ from -0.5 to 0 can result in a 9 orders of magnitude change in the overall collision frequency. This effect is commensurate with the log-linear relationship between μ and ρ and why we observe a 9 order of magnitude change in c between $\rho = 0$ and $\rho = 0.5$. For the variation in τ, the electron temperature coefficient, the inverse dependence on electron temperature is what places the local minimum.[29] Therefore, increasing the value is expected to produce a sharper local minimum, which requires variation in c to increase the minimum to the "true" value.

E. Limitations of form for closure model

The largest shortcoming of the model is its inability to simultaneously place the ion velocity and electron temperature curves in line with experimental data. This issue can be seen in the plots of the TR and IVR in Figs. 3 and 7 as the parameter set that minimizes IVR maximizes TR. Likewise, while the neutral density variation is able to capture the peak temperature, it produces a larger IVR and more shallow acceleration than the plasma density case. Overall, these results suggest that the electron temperature is too large downstream of the acceleration region. The likely explanation for this behavior is the electric field is too large in this region, which artificially inflates Ohmic heating of the electrons. Follow on efforts could center on identifying plasma dependencies for the closure model that would reduce the electric field in this area.

A final discrepancy we note is in the divergence efficiency as all cases presented were unable to match the experimental value. While this discrepancy is notable, we believe it to be a symptom of the inability to fully place the ion acceleration. That is, when more acceleration occurs further back in the channel, the ion beam is more collimated. For example, the $\mu = 2.0$ case in Figs. 3 and 4 overpredicts the divergence efficiency when it correctly places the ion acceleration upstream. Physically, when slower ion acceleration occurs, the ions spend more time in regions with radial electric fields that produce divergence. Therefore, we expect that should the ion velocity profile be fully matched, the discrepancy with divergence efficiency would be resolved.

VI. Conclusion

In this work we employed a self-consistent algebraic closure based on a product of plasma density, neutral density, and electron temperature in a Hall thruster model. The electron energy equation was closed using an adiabatic heat flux along field lines. It was found that by adjusting the dependence on plasma and neutral density we are able to capture the peak temperature, global performance metrics and qualitatively the spatial dependence in the ion acceleration. This result thus represents additional progress on demonstrating the ability of simple closures when paired with a modified version for the energy transport in these systems

can approach accurate predictions of experimental data. With that said, we have found the closure model has shortcomings, most notably in its inability to correctly capture the location of the ion velocity curve and electron temperature. This suggests that the model may be incomplete with the need to introduce additional dependencies on the background plasma properties. This work has broader implications for the field as it highlights the importance of evaluating performance metrics and including neutral interactions when evaluating closures of the anomalous collision frequency.

Acknowledgments

This work was supported in part by a NSF GRFP, the NASA Joint Advance Propulsion Institute (80NSSC21K1118), DOE grant DE-SC0022988, and computational resources provided by Advanced Research Computing at the University of Michigan. The authors would also like to thank Madison Allen and John Riley O'Toole for insightful discussion.

References

[1]Lev, D., Myers, R. M., Lemmer, K. M., Kolbeck, J., Koizumi, H., and Polzin, K., "The technological and commercial expansion of electric propulsion," *Acta Astronautica*, Vol. 159, 2019, pp. 213–227.

[2]Snyder, J. S., Lopez Ortega, A., Mikellides, I. G., Li, J., Murphy, A., and Johnson, I., "Electric Propulsion for the Psyche Mission: A new trajectory and final preparations for launch," *AIAA SCITECH 2024 Forum*, Vol. AIAA 2024-1958, January 2024.

[3]Villafana, W., Powis, A. T., Kaganovich, I. D., Khrabrov, A., and Ethier, S., "Algorithms and High-Performance Computing for Kinetic Electric Propulsion Simulations," *38th International Electric Propulsion Conference*, Electric Rocket Propulsion Society, Toulouse, France, 2024, Paper no. 748.

[4]Marks, T. A. and Gorodetsky, A., "GPU-accelerated kinetic Hall thruster simulations in WarpX," *Journal of Electric Propulsion*, 2025.

[5]Chen, X., Xie, L., Zhong, K., Luo, X., Zhou, Z., Wang, B., Liu, Z., and Zhao, Y., "Influence of plume region arrangement on Hall thruster azimuthal instability: 3D PIC simulations via a newly developed code PMSL-PIC-HET-3D," *Physics of Plasmas*, Vol. 32, No. 5, 05 2025, pp. 052103.

[6]Davidson, R. and Krall, N., "Anomalous transport in high-temperature plasmas with applications to solenoidal fusion systems," *Nuclear Fusion*, Vol. 17, No. 6, dec 1977, pp. 1313.

[7]Fife, J. M., *Hybrid-PIC Modeling and Electrostatic Probe Survey of Hall Thruster*, Ph.D. thesis, Massachusetts Institute of Technology, 1998.

[8]Morozov, A. I. and Savel'ev, V. V., *Reviews of Plasma Physics*, Vol. 21, Kluwe Academic/Plenum Publisers, 2000.

[9]Boeuf, J. P. and Garrigues, L., "Low frequency oscillations in a stationary plasma thruster," *Journal of Applied Physics*, Vol. 84, No. 7, 10 1998, pp. 3541–3554.

[10]Cappelli, M., Meezan, N., and Gascon, N., "Transport physics in Hall plasma thrusters," *40th AIAA Aerospace Sciences Meeting & Exhibit*, 2002.

[11]Scharfe, M. K., Thomas, C. A., Scharfe, D. B., Gascon, N., Cappelli, M. A., and Fernandez, E., "Shear-Based Model for Electron Transport in Hybrid Hall Thruster Simulations," *IEEE Transactions on Plasma Science*, Vol. 36, No. 5, 2008, pp. 2058–2068.

[12]Chodura, R., Bardotti, G., and Engelmann, F., "Numerical investigation of the anomalous resistivity due to two-stream instability," *Plasma Physics*, Vol. 13, No. 12, dec 1971, pp. 1099.

[13]Cappelli, M. A., Young, C. V., Cha, E., and Fernandez, E., "A zero-equation turbulence model for two-dimensional hybrid Hall thruster simulations," *Physics of Plasmas*, Vol. 22, No. 11, 11 2015, pp. 114505.

[14]Jorns, B. A., "Two Equation Closure Model for Plasma Turbulence in a Hall Effect Thruster," *36th International Electric Propulsion Conference*, Electric Rocket Propulsion Society, Vienna, Austria, Sept. 2019.

[15]Mikellides, I. G., Jorns, B., Katz, I., and Ortega, A. L., "Hall2De Simulations with a First-principles Electron Transport Model Based on the Electron Cyclotron Drift Instability," *52nd AIAA/SAE/ASEE Joint Propulsion Conference*, 2016.

[16]Lafleur, T., Baalrud, S. D., and Chabert, P., "Theory for the anomalous electron transport in Hall effect thrusters. II. Kinetic model," *Physics of Plasmas*, Vol. 23, No. 5, 05 2016, pp. 053503.

[17]Marks, T. A. and Jorns, B. A., "Evaluation of algebraic models of anomalous transport in a multi-fluid Hall thruster code," *Journal of Applied Physics*, Vol. 134, No. 15, 10 2023, pp. 153301.

[18]Mikellides, I. G., Lopez Ortega, A., and Chaplin, V. H., "Theory of the anomalous momentum exchange from wave–particle interactions in Hall-effect ion accelerators and comparisons with measurements," *Physics of Fluids*, Vol. 36, No. 7, 07 2024, pp. 074121.

[19]Kwon, K., "Analytical modeling of the anomalous electron collision frequency in partially magnetized E × B plasmas," *AIP Advances*, Vol. 11, No. 8, 08 2021, pp. 085324.

[20]Jorns, B., "Predictive, data-driven model for the anomalous electron collision frequency in a Hall effect thruster," *Plasma Sources Science and Technology*, Vol. 27, No. 10, oct 2018, pp. 104007.

[21]Roberts, P. J., Allen, M. G., Brick, D. G., and Jorns, B. A., "Empirical Closures for Momentum and Energy Transoprt in Hall Thrusters based on Thomson Scattering Measurements," *38th International Electric Propulsion Conference*, Electric Rocket Propulsion Society, Toulouse, France, 2024, Paper no. 393.

[22]Vincent, B., Tsikata, S., and Mazouffre, S., "Incoherent Thomson scattering measurements of electron properties in a conventional and magnetically-shielded Hall thruster," *Plasma Sources Science and Technology*, Vol. 29, No. 3, mar 2020, pp. 035015.

[23]Roberts, P. J. and Jorns, B. A., "Laser Measurement of Anomalous Electron Diffusion in a Crossed-Field Plasma," *Phys. Rev. Lett.*, Vol. 132, Mar 2024, pp. 135301.

[24]Betancourt, J. L. S., Butler-Craig, N., Lopez-Uricoechea, J., Steinberg, A. M., and Walker, M. L. R., "Laser Thomson scattering measurements indicate non-isothermal magnetic field lines in magnetically shielded Hall effect thrusters," *Physics of Plasmas*, Vol. 31, No. 11, 11 2024, pp. 113106.

[25]Roberts, P. J., *Characterization of Momentum and Heat Flow in Hall Thrusters with Laser Scattering*, Ph.D. thesis, University of Michigan, 2025.

[26]Lopez-Uricoechea, J., Suazo Betancourt, J. L., Butler-Craig, N., and Walker, M. L., "Laser Thomson Scattering Measurements and Inference of the Electron Hall Parameter Across the Acceleration Region of a Hall Effect Thruster," *38th International Electric Propulsion Conference*, Electric Rocket Propulsion Society, Toulouse, France, 2024, Paper no. 509.

[27]Brick, D. G., Roberts, P. J., and Jorns, B. A., "Model Based Investigation of Anomalous Energy Transport in a Magnetically-Shielded Hall Thruster," *38th International Electric Propulsion Conference*, Electric Rocket Propulsion Society, Toulouse, France, 2024, Paper no. 411.

[28]Brick, D., Roberts, P., and Jorns, B., "On the Adiabatic Nature of Electron Energy Transport Along Magnetic Field Lines in Hall Thrusters," *In preparation*.

[29]Brick, D. G., Roberts, P. J., and Jorns, B. A., "Numerical Investigation of Electron Energy Transport in Hall Thrusters," *2025 AIAA SciTech Forum and Exposition*, AIAA, 2025.

[30]Katz, I. and Mikellides, I. G., "Neutral gas free molecular flow algorithm including ionization and walls for use in plasma simulations," *Journal of Computational Physics*, Vol. 230, No. 4, 2011, pp. 1454–1464.

[31]Mikellides, I. G. and Katz, I., "Numerical simulations of Hall-effect plasma accelerators on a magnetic-field-aligned mesh," *Phys. Rev. E*, Vol. 86, Oct 2012, pp. 046703.

[32]Lopez Ortega, A. and Mikellides, I. G., "A New Cell-Centered Implicit Numerical Scheme for Ions in the 2-D Axisymmetric Code Hall2De," *50th AIAA/ASME/SAE/ASEE Joint Propulsion Conference*, 2014.

[33]Lopez Ortega, A. and Mikellides, I. G., "The importance of the cathode plume and its interactions with the ion beam in numerical simulations of Hall thrusters," *Physics of Plasmas*, Vol. 23, No. 4, 04 2016, pp. 043515.

[34]Ortega, A. L., Mikellides, I. G., Chaplin, V. H., Huang, W., and Frieman, J. D., "Anomalous Ion Heating and Pole Erosion in the 12.5-kW Hall Effect Rocket with Magnetic Shielding (HERMeS)," *AIAA Propulsion and Energy 2020 Forum*, 2020.

[35]Mikellides, I. G., Katz, I., Goebel, D. M., and Polk, J. E., "Hollow cathode theory and experiment. II. A two-dimensional theoretical model of the emitter region," *Journal of Applied Physics*, Vol. 98, No. 11, 12 2005, pp. 113303.

[36]Su, L. L. and Jorns, B. A., "Performance comparison of a 9-kW magnetically shielded Hall thruster operating on xenon and krypton," *Journal of Applied Physics*, Vol. 130, No. 16, 10 2021, pp. 163306.

[37]Georgin, M. P., Jorns, B. A., and Gallimore, A. D., "Transient non-classical transport in the hollow cathode plume I: measurements of time-varying electron collision frequency," *Plasma Sources Science and Technology*, Vol. 29, No. 10, oct 2020, pp. 105010.

[38]Spitzer, L. and Harm, R., "Transport Phenomena in a Completely Ionized Gas," *Phys. Rev.*, Vol. 89, Mar 1953, pp. 977–981.

[39]Braginskii, S., "Transport Processes in a Plasma," *Reviews of Plasma Physics*, Vol. 1, 1965, pp. 205–311.

[40]Domínguez-Vázquez, A., *Axisymmetric simulation codes for Hall effect thrusters and plasma plumes*, Ph.D. thesis, Universidad Carlos III de Madrid, 2019.

[41]Shashkov, A., Lovtsov, A., Tomilin, D., and Kravchenko, D., "Numerical study of viscosity and heat flux role in heavy species dynamics in Hall thruster discharge," *Plasma Science and Technology*, Vol. 25, No. 1, nov 2022, pp. 015511.

[42]Sahu, R., Mansour, A. R., and Hara, K., "Full fluid moment model for low temperature magnetized plasmas," *Physics of Plasmas*, Vol. 27, No. 11, 11 2020, pp. 113505.

[43]Hagelaar, G. J. M., Bareilles, J., Garrigues, L., and Boeuf, J. P., "Two-dimensional model of a stationary plasma thruster," *Journal of Applied Physics*, Vol. 91, No. 9, 05 2002, pp. 5592–5598.

[44]Parra, F. I., Ahedo, E., Fife, J. M., and Martínez-Sánchez, M., "A two-dimensional hybrid model of the Hall thruster discharge," *Journal of Applied Physics*, Vol. 100, No. 2, 07 2006, pp. 023304.

[45]Poli, D., Bello-Benítez, E., Fajardo, P., and Ahedo, E., "Time-dependent axial fluid model of the Hall thruster discharge and its plume," *Journal of Physics D: Applied Physics*, Vol. 56, No. 41, jul 2023, pp. 415203.

[46]Ahedo, E., Gallardo, J. M., and Martinez-Sanchez, M., "Model of the plasma discharge in a Hall thruster with heat conduction," *Physics of Plasmas*, Vol. 9, No. 9, 09 2002, pp. 4061–4070.

[47]Tsikata, S., Lemoine, N., Pisarev, V., and Grésillon, D. M., "Dispersion relations of electron density fluctuations in a Hall thruster plasma, observed by collective light scattering," *Physics of Plasmas*, Vol. 16, No. 3, 03 2009, pp. 033506.

[48]Brown, Z. A. and Jorns, B. A., "Growth and Saturation of the Electron Drift Instability in a Crossed Field Plasma," *Phys. Rev. Lett.*, Vol. 130, Mar 2023, pp. 115101.

[49]Cavalier, J., Lemoine, N., Bonhomme, G., Tsikata, S., Honoré, C., and Grésillon, D., "Hall thruster plasma fluctuations identified as the E×B electron drift instability: Modeling and fitting on experimental data," *Physics of Plasmas*, Vol. 20, No. 8, 08 2013, pp. 082107.

[50]Ducrocq, A., Adam, J. C., Héron, A., and Laval, G., "High-frequency electron drift instability in the cross-field configuration of Hall thrusters," *Physics of Plasmas*, Vol. 13, No. 10, 10 2006, pp. 102111.

[51]Janhunen, S., Smolyakov, A., Chapurin, O., Sydorenko, D., Kaganovich, I., and Raitses, Y., "Nonlinear structures and anomalous transport in partially magnetized E×B plasmas," *Physics of Plasmas*, Vol. 25, No. 1, 12 2018, pp. 011608.

[52]Villafana, W., Cuenot, B., and Vermorel, O., "3D particle-in-cell study of the electron drift instability in a Hall Thruster using unstructured grids," *Physics of Plasmas*, Vol. 30, No. 3, 03 2023, pp. 033503.

[53]Liu, M. F. and Jorns, B. A., "Experimental Measurements of the Dispersion and Growth Rate of Ion Acoustic Waves in the Plume of a Hollow Cathode," *38th International Electric Propulsion Conference*, Electric Rocket Propulsion Society, Toulouse, France, 2024, Paper no. 366.

[54]Mikellides, I. G. and Lopez Ortega, A., "Challenges in the development and verification of first-principles models in Hall-effect thruster simulations that are based on anomalous resistivity and generalized Ohm's law*," *Plasma Sources Science and Technology*, Vol. 28, No. 1, jan 2019, pp. 014003.

[55]Su, L. L., Marks, T. A., and Jorns, B. A., "Investigation into the efficiency gap between krypton and xenon operation on a magnetically shielded Hall thruster," *37th International Electric Propulsion Conference*, Electric Rocket Propulsion Society, Boston, Massachusetts, 2024.

[56]Marks, T. A., *Modeling Anomalous Electron Transport in a Fluid Hall Thruster Code*, Ph.D. thesis, University of Michigan, 2023.

[57]Dragnea, H. C., Ortega, A. L., Kamhawi, H., and Boyd, I. D., "Simulation of a Hall Effect Thruster Using Krypton Propellant," *Journal of Propulsion and Power*, Vol. 36, No. 3, 2020, pp. 335–345.